IAEA nuclear fusion

PAPER • OPEN ACCESS

# Impact of the JET ITER-like wall on H-mode plasma fueling

To cite this article: S. Wiesen *et al* 2017 *Nucl. Fusion* **57** 066024

OPEN ACCESS
IOP Publishing | International Atomic Energy Agency
Nuclear Fusion
Nucl. Fusion **57** (2017) 066024 (9pp)
https://doi.org/10.1088/1741-4326/aa69dd

# Impact of the JET ITER-like wall on H-mode plasma fueling

**S. Wiesen[1], S. Brezinsek[1], M. Wischmeier[2], E. De la Luna[3], M. Groth[4], A. E. Jaervinen[5], E. de la Cal[3], U. Losada[3], A.M. de Aguilera[3], L. Frassinetti[6], Y. Gao[1,7], C. Guillemaut[8], D. Harting[9], A. Meigs[9], K. Schmid[2], G. Sergienko[1] and JET contributors[a]**

EUROfusion Consortium, JET, Culham Science Centre, Abingdon, OX14 3DB, United Kingdom
[1] Forschungszentrum Jülich GmbH, Institut für Energie- und Klimaforschung—Plasmaphysik, Partner of the Trilateral Euregio Cluster (TEC), 52425 Jülich, Germany
[2] Max-Planck-Institut für Plasmaphysik, 85748 Garching bei München, Germany
[3] Laboratorio Nacional de Fusion, CIEMAT, 28040, Madrid, Spain
[4] Aalto University, Otakaari, Espoo, Finland
[5] Lawrence Livermore National Laboratory, Livermore, CA 94550, United States of America
[6] Association VR, Fusion Plasma Physics, KTH, SE-10044 Stockholm, Sweden
[7] Institute of Plasma Physics, Chinese Academy of Sciences, Hefei 230031, People's Republic of China
[8] Instituto de Plasmas e Fusão Nuclear, IST, Univ. de Lisboa, P-1049-001, Lisboa, Portugal
[9] CCFE, Culham Science Centre, Abingdon OX14 3DB, United Kingdom

E-mail: s.wiesen@fz-juelich.de

Received 15 December 2016, revised 24 March 2017
Accepted for publication 29 March 2017
Published 26 April 2017

**Abstract**

JET ITER-like wall (ILW) experiments show that the edge density evolution is strongly linked with the poloidal distribution of the ionization source. The fueling profile in the JET-ILW is more delocalized as compared to JET-C (JET with carbon-based plasma-facing components PFCs). Compared to JET-C the H-mode pedestal fueling cycle is dynamically influenced by a combination of plasma–wall interaction features, in particular: (1) edge-localized modes (ELMs) induced energetic particles are kinetically reflected on W divertor PFCs leading to distributed refueling away from the divertor depending on the divertor plasma configuration, (2) delayed molecular re-emission and outgassing of particles being trapped in W PFCs (bulk-W at the high field side and W-coated CFCs at the low field side) with different fuel content and (3) outgassing from Be co-deposits located on top of the high-field side baffle region shortly after the ELM. In view of the results of a set of well diagnosed series of JET-ILW type-I ELMy H-mode discharges with good statistics, the aforementioned effects are discussed in view of H-mode pedestal fueling capacity. The ongoing modelling activities with the focus on coupled core-edge plasma simulations and plasma–wall interaction are described and discussed also in view of possible code improvements required.

Keywords: H-mode, JET, ITER-like wall, integrated modelling, pedestal fuelling, plasma–wall interaction



[a] See the author list of 'Overview of the JET results in support to ITER' by Litaudon *et al* to be published in *Nuclear Fusion* Special issue: overview and summary reports from the *26th Fusion Energy Conf. (Kyoto, Japan, 17–22 October 2016)*

 

## 1. Introduction

The JET ILW consists of a beryllium first-wall and tungsten armor in the divertor [1] and has demonstrated to perform very successfully for plasma–wall interaction (PWI) and plasma operation with the plasma-facing material selection foreseen in ITER [2]. The JET-ILW demonstrated the low expected long-term fuel retention in the metallic environment (factor 10–15 less than JET-C) predominantly due to co-deposition in Be and about 1/3 due to implantation and surface coverage in Be and W [3, 4] as well as allows fast isotope exchange of the accessible reservoir in the PFCs which is about 1/10 of the one in JET-C [5, 6]. As for JET-C stiff transport determines the evolution of the central density in a tokamak plasma and is thus mainly driven by the edge pedestal height if not otherwise fueled by pellet ablation. Initial comparisons of JET-ILW with JET-C (JET with PFCs made of carbon-fiber composites) showed that the evolution of the edge density is strongly linked with the level of recycling [7] as with increasing density a delay is observed before the pedestal density recovers after an ELM-crash. As a consequence a degraded confinement $H_{98,y} < 1.0$ is generally observed in high current unseeded baseline scenarios as an increased density enforced by deuterium fueling is required to avoid tungsten accumulation. To mitigate the reduced confinement divertor plasma configurations with the strike-lines close to the divertor corners are preferred as pumping is enhanced [8] to allow for better particle control and, as a side effect, direct reflection of sputtered W into the confined region is partly inhibited. Moving from a semi-horizontal divertor configuration to a vertical or corner configuration in JET usually also means a significant increase of the plasma clearance towards the HFS baffle region and thus decreases any impact of far-SOL recycling effects on the fueling.

The pre-ELM pedestal width $\Delta n_{\mathrm{ped}}$ and height $n_{\mathrm{ped}}$ is significantly influenced by the poloidal and radial ionization profile just inside the separatrix. Regression analysis of JET-ILW H-mode pedestal profiles revealed recently that $\Delta n_{\mathrm{ped}}$ depends on pedestal collisionality $\nu^{*}_{\mathrm{ped}}$ [9]. Indeed, the number of deuterium ionized close to the separatrix depends directly on the global particle flux balance within the scrape-off layer (SOL) and is a function of neutral and plasma transport as well as PWI. During JET-C operation, the recycled deuterium flux in the divertor typically dominated the externally applied gas flux and the neutrals cross dominantly the X-point region from the divertor region to refuel the plasma core. As a consequence from such a localized particle source, reliable predictions of the pedestal performance by using edge stability models like EPED [10] were possible leading to the peeling–ballooning (P–B) scaling for $\Delta n_{\mathrm{ped}} \sim \sqrt{\beta_{\mathrm{pol,ped}}}$ in carbon devices. Albeit the impact of neutral penetration and de-localised recycling patterns on $n_{\mathrm{ped}}$ and $\Delta n_{\mathrm{ped}}$ had been conjectured very early in analytical models [11] and by using coupled 1D plasma-neutral models [12], deviations from the aforementioned P–B paradigm are often and tersely referred to as ‘atomic physics effects’ by some authors (e.g. Maggi *et al* [13]) and are subsequently treated as unknown model parameters.

With the installation of the JET-ILW it has become even more evident that an oversimplified neutral model is insufficient to find a scaling for the pedestal structure. In fact, the impact of the metallic wall on the fueling process has been recovered very early during the first JET-ILW campaigns as the poloidal distribution of the ionization source and the fueling profile have become more delocalized (i.e. away from the divertor). For example from L-mode discharges in low-recycling conditions [14] one can estimate that the ratio of injected particles $\Gamma_{\mathrm{inj}}$ to the total recycling flux $\Gamma_{\mathrm{rec}}$ is of order 3–5 higher in JET-ILW than in JET-C (with $\Gamma_{\mathrm{rec}}$ being derived from $D_{\alpha}$ radiation photon emission fluxes converted into a recycling flux using integral S/XB values [15]). In H-mode this ratio can be even larger as energetic particles can enter deeper into the metallic bulk-W/W-coated CFC surface layers in the divertor so that for achieving a given pedestal density $n_{\mathrm{ped}}$ a throughput of one order of magnitude higher is required in JET-ILW than without carbon. The additional D particle source due to chemical erosion of thick amorphous carbon (a-C:D) layers with high fuel content (C:D in the average of 0.5) is effectively switched off (compared to a similar JET-C discharge 15 times less residual C is abundant in JET-ILW).

During the JET-ILW campaigns it has been more and more recognized that, in comparison to JET-C operation, other pronounced features may have an impact on the H-mode fueling cycle dynamics during and between ELMs. Some specific physical mechanisms in the evolution of the global particle balance have become more relevant. In particular, the poloidal fueling profile is dynamically influenced by the following PWI effects:

1. ELM induced energetic particles with up to 4–5 times equivalent to pedestal temperature [16] are kinetically reflected on metallic W divertor PFCs leading to a more distributed refueling away from the divertor. For example, the particle reflection coefficient for a D-particle with 1 keV impact energy increases from 0.1 to 0.5 when moving from C to W and likewise, the energy reflection coefficient increases by one order of magnitude [17]. This induces the kinetic-geometric effect of reflected particles amending the poloidal ionization source profile (see figure 1). Depending on the divertor plasma shape (e.g. horizontal versus vertical target or corner configuration) recycled neutral molecules and atoms reach the private or common flux zone where they are dissociated and ionized, or, pumped away as particles may or may not reach the pump ducts more easily.
2. Molecular re-emission can be delayed as particles can be trapped in W PFCs, bulk-W and W-coated CFCs with different fuel content, resulting in retarded recycling after the ELM due to surface temperature $T_{\mathrm{surf}}$ dependent outgassing effects and heat diffusion into near surface layer ($\mu$m) [18].
3. At the main-chamber wall Be is eroded and material migration leads to deposition of Be predominantly on the upper inner target plate [19]. Re-erosion and multistep transport along the target plate as in JET-C does not take place due to absence of chemical erosion at low impact

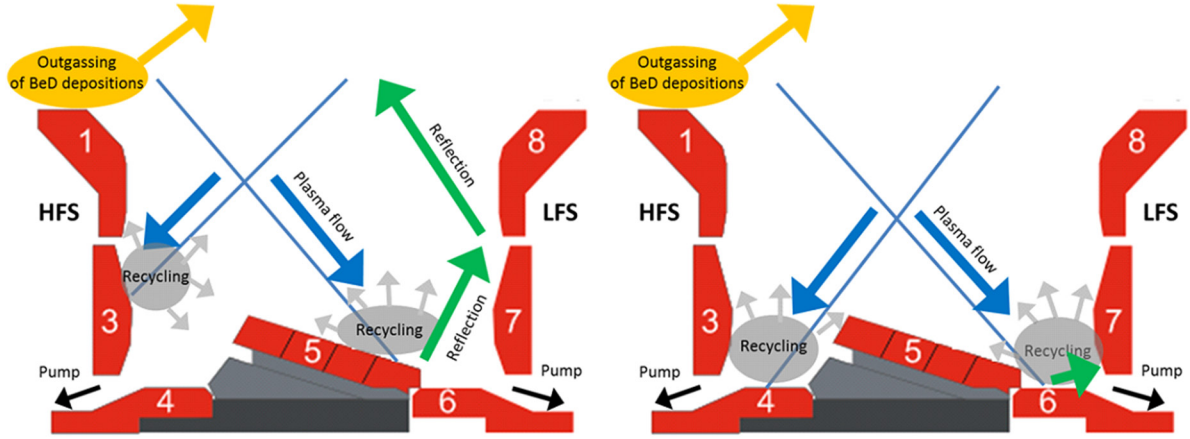


**Figure 1.** Schematic view of particle recycling during the ELM leading to a delocalised poloidal fueling profile. Left: semi-horizontal configuration. Right: corner configuration.

energy [20]. It was found in JET that during the ELM significant outgassing does occur from these deposition areas leading to a localized fueling effect on the high-field side (HFS). Compared to the LFS outgassing from bulk-W PFCs, the impact of the HFS outgassing on the poloidal fueling profile may be larger as the porous near-surface deposition layers on top of W-coated PFCs allow for a larger particle reservoir (factor ~20).

4. Nitrogen seeding (or hydrocarbons $C_xD_y$) may lead to the formation of surface chemical compounds which can store temporarily D particles in the wall and other chemical transport channels come into play (e.g. due to formation of ammonia or carbon co-deposits at the wall).

In this paper we focus on point 2 and 3. The impact of kinetic effects on recycling and W sputtering has been dealt with by other authors already [16, 21] as well as the impact of the selection of the divertor configuration [8, 22]. Generally the neutral kinetics effects are already included being an essential part of the fluid-kinetic edge transport codes like SOLPS-ITER [23] or EDGE2D-EIRENE [24, 25]. A discussion on the effect of an increase in particle and energy reflectivity in case of the JET-ILW has been addressed also in [47]. The impact of nitrogen on confinement is being dealt with in a separate contribution [26].

## 2. Experimental results

In this paper we present results from dedicated JET-ILW H-mode experiments in 2012 (during the JET-ILW C30C campaign [3]) with $I_p/B_t = 2.0$ MA/2.0 T, low-triangularity, auxiliary neutral beam injection $P_{NBI} = 11$ MW in semi-horizontal divertor configurations with typical thermal energy drops of 160 kJ per ELM. The experiments focused on the 'footprint in material migration and retention' and the assessment of recycling behavior as well as outgassing effects. The ELMs appeared in 6 s long flattop phases of the discharges with frequency of about 30 Hz. The gas injection rate was in the order of $1.0 \times 10^{22}$ D $s^{-1}$ into the divertor feed-forward with active cryo-pumps. The magnetic configuration in the plasma series (accumulated 900 s in H-mode) on semi-horizontal configuration, i.e. the inner strike point (ISP) on vertical target (tile 3), W-coated CFC) and outer strike point (OSP) on the bulk-W divertor target plate (tile 5). The strike lines were static and positioned to identify well defined surface temperatures $T_{surf}$ measured by the JET divertor IR system [27].

Figure 2 depicts coherently averaged outer-midplane $n_e$ and $T_e$ profiles taken from the high-resolution Thomson scattering system (HRTS) for the times: just before an ELM-crash (0 ms), shortly after the ELM with maximum drop in pedestal pressure (1.2 ms) and just before recovery (5.6 ms) at which point the $n_e$ profile has just reached its minimum and starts to recover. At that time $T_e$ has already started to increase which is mainly driven by the power entering the pedestal from the plasma core. Such a delayed recovery of the density after the ELM was not observed in JET-C with much shorter ELM cycles. Figure 2 also displays coherently averaged fits [28] of the pedestal structure, i.e. widths and heights, as function of time during the ELM crash. Clearly, secondary drops are observed in both $n_{ped}$ and $T_{ped}$ about 6–9 ms after the ELM. $\Delta n_{ped}$ increases after the initial $n_{ped}$ drop from 2 cm to 4.5 cm and increases even further to ~6 cm until $n_{ped}$ recovery is briefly hampered at the point $T_{ped}$ has reached its first maximum at about 5 ms. It takes another drop in $T_{ped}$ and further reduction in $\Delta T_{ped}$ to allow the density to come up to its original value after 15–20 ms. $\Delta T_{ped}$ and $\Delta n_{ped}$ have shrunk to their original value already at 10 ms after the ELM.

The recycling flux close to the divertor target plates was measured by Langmuir probes as well as spectroscopically by deuterium Balmer-$\alpha$ and molecular emission of the Fulcher band [15]. A spectroscopic camera was used to discriminate the $D_\alpha$ and WI emission on the HFS top and bottom divertor during the ELM and in the inter-ELM period [29].

## 3. Fast outgassing from bulk-W/W-coated CFC

The impact of retention, desorption and recycling during the ELM on the divertor conditions has been addressed in [18] for the same set of discharges. ELM-induced desorption from saturated near-surface layers and implantation W regions as well as deep ELM-induced deuterium implantation under

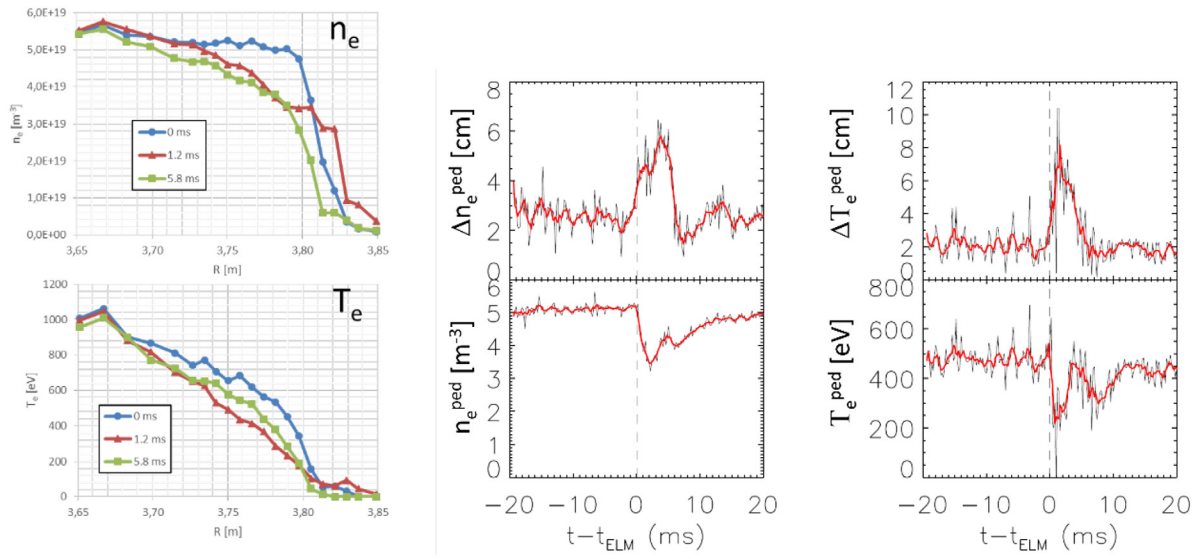


**Figure 2.** Left: coherently averaged HRTS profiles of pedestal density and temperature before the ELM (0 ms), with maximum drop in $p_{ped}$ (1.2 ms) and during the recovery phase (5.8 ms). Right: pedestal structure fits of coherently averaged type-I ELM-events: pedestal widths $w_{ne}$ and $w_{Te}$ and heights $n_{ped}$ and $T_{ped}$ as a function of time. Clearly, secondary drops are observed in both $n_{ped}$ and $T_{ped}$ about 6–9 ms after the ELM.

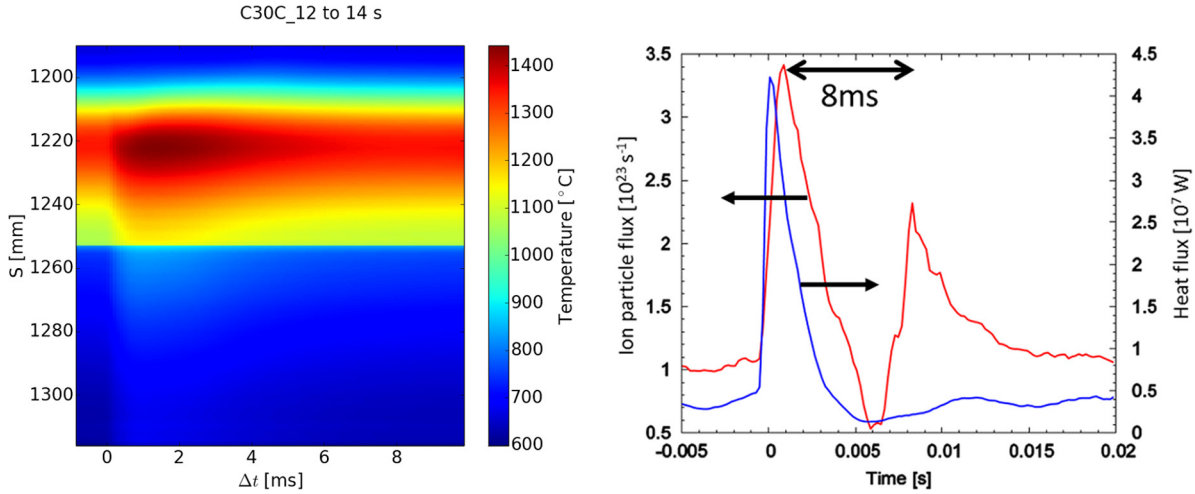


**Figure 3.** Evolution of a typical type-I ELM event of the 2012 campaign incl. pre/post phase ELM (coherently averaged LFS profiles over many ELMs of identical discharges), left: $T_{surf}$ evolution derived from IR thermography ($S$-coordinate along plate), right: integrated signals (along $S$-coordinate) of the coherently averaged heat flux arriving at the plate derived from IR measurements and ion particle flux from Langmuir probe saturation current (reprocessed data from [46], it is assumed that the flux footprints are toroidally symmetric). Clearly, a $\Delta t \sim 8$ ms delay between primary and secondary peak in the ion flux is observed.

varying baseline temperature conditions at the bulk-W tile takes place as during the discharge $T_{surf}$ rises from a base level of about 160 °C exceeding up to 1400 °C at the end of the flattop phase close to the OSP. The temporal and spatial evolution of $T_{surf}$ of a set of coherently averaged ELM bursts is depicted in figure 3. About 1600 individual ELM footprints taken from the last 2.0 s of the flattop phase during the discharges with $T_{surf} > 800$ °C where the temporal ELM footprint evolution appears self-similar. Also shown in figure 3 are the coherently averaged evolutions of the heat-flux density profiles measured by the IR system as well as the saturation current profiles along the horizontal target plate. The initial particle flux peak occurs almost at the same time with the ELM driven heat flux arriving at the plate. The slower convective nature of particle transport compared to the fast heat conduction is likely responsible for a slight delay of about 1 ms. One can clearly identify a second pronounced peak in the $J_{sat}$ signal about $\Delta t \sim 8$ ms after the first particle flux peak which has not been observed in JET-C. Typically in JET-ILW, this secondary peak has no correspondence to the impinging Be ion flux and the W sputtering influx [30] which indicates that the secondary peak is not related to ions from the pedestal region (having large energies [16]) as it occurs already well within the slow recovery phase of the pedestal. Also the impact energy must be low as no W sputtering by Be or D occurs at the point of the second peak (W sputter threshold at 60 eV for Be ions and 300 eV for D ions [2]). The coherent appearance of both impinging ions ($J_{sat}$) and $D_\alpha$

radiation suggests that the origin of the second peak is related to a temporary appearance of localized recycling (low energy) at the target plate.

The aforementioned observations are based on data gathered from the last 2.0 s part of the flattop phase of the discharges only. In this phase $T_{surf}$ has saturated in the region 1200 °C -1400 °C. However, the ELM signature has already been found to be strongly dependent on $T_{surf}$ [18]. Specifically, the peak W surface temperature exhibits a qualitative change in the temporal signature (see figure 3 in [18]). At the lowest accessible surface temperatures ($T_{surf} = 300$ °C $< 450$ °C) the ELM footprints show the shortest ELM duration and the signatures look clean, similar to the ELMs found in JET-C. However, at surfaces temperatures above a given threshold $T_{surf} > 500$ °C the ELM signatures become different. In the beginning of the ELM the typical temperature rise of about 100 °C when the heat load arrives at the plate, but afterwards a pronounced drop in temperature after the end of the ELM crash is observed. This drop is caused by local plasma cooling due to enhanced $D_2$ desorption at $T_{surf} > 500$ °C at the bulk-W PFC which reduces the inter-ELM heat load reaching the plate before the next ELM occurs. Outgassing, which is governed by diffusion of particles out of the W PFC surface, is quite localized in radial direction and depends on the fuel content in the W surface layers as well as $T_{surf}$. By increasing $T_{surf}$ even further (the PFCs are inertially cooled) the desorption of $D_2$ is reduced again as less D particles can be stored in the W surface.

The process of outgassing can be described by trap-diffusive models as described for example in [31]. These models must make assumptions about the impinging heat and particle flux as well as about the concentration of trap locations in the W or Be material solute. With the coherently averaged transients for particle and heat flux footprints of the discharges, the derived recycling coefficient during the ELM $R^{ELM}$ can be of the order unity [31]. The trap-concentration in W or W-coated CFC materials can be as high as 10% within the first couple of $\mu$m [32]. With this high level of trap-concentration in the W-solute the calculated ratio $\xi =$ effusing/implanted flux may vary between 0.4–2.0. Subsequently, by assuming a particle reflection coefficient of ~0.5 for 1 keV D-particles on W-PFC [17] and for the $\xi \sim 0.5$ one derives an effective recycling coefficient $R_{ELM} \sim 0.75$ [33].

The JINTRAC integrated model [34] is a self-consistent approach of coupling the 1D core/pedestal transport code JETTO with the 2D edge plasma/PWI code EDGE2D-EIRENE. It has been employed to assess the impact of recycling conditions for the discussed type-I ELM discharges [35]. For the analysis in [35] a new but very simple dual-reservoir model has been introduced into the EDGE2D-EIRENE coupling (part of the JINTRAC code suite). It allows a particle reservoir for each HFS and LFS target plates of finite size which has been set to the order of $10^{20}$ particles (in [35] a sensitivity study of the actual near-surface particle reservoir capacity has been executed neglecting any in-out asymmetry in the chosen reservoir sizes). In the short time between reservoir emptying (after an individual ELM-burst arrived at the target plate) and replenishing the reservoir by the impinging target particle flux, the recycling coefficient $R^{ELM}$ has been reduced to values between 0.3 and 0.5. Outside this short phase lasting a couple of ms (depending on the finite reservoir size) the recycling coefficient has been set back to unity. This model setup is oversimplified as it ignores the $T_{surf}$ dependency on $R^{ELM}$ and reservoir size, however it does show a delayed recovery of the pedestal density of the order of 10 ms, see results presented in [35]. The model does not recover the slow response of $T_{ped}$ on the ELM as, for example, expected from the experiment [7, 36], see also figure 2 (right). It is very likely that other effects like a change in MHD stability after the ELM (as response to changes for example in separatrix or fueling conditions) do play an important role in the recovery of $T_{ped}$, too. It should be noted that the pedestal transport model in JINTRAC also does not include yet a coupling of density and temperature as for example demanded by [37] and other authors. The JINTRAC model as described in [35] also does not reproduce the secondary peak in the recycling flux 8 ms after the ELM. Obviously, there are other features missing in the model which are required to track those recycling transients. In the following section some of the missing model constraints are discussed which are consistent with the idea of an extended (non-local) reservoir model.

## 4. Outgassing from Be co-deposits during ELM at the HFS

In the JET-ILW the major fraction of eroded Be particles from the main-chamber are co-deposited near or on top the HFS baffle region [19] (see figure 1, tile 1). Post-mortem analysis of the deposits after the first JET-ILW campaigns showed that about 1/3 of global fuel retention was located on HFS tile 1 and tile 0 (high-field gap closure tile) with D (or H) particles stored within the 40 $\mu$m thick co-deposited layers (SIMS analysis [38]). In such co-deposits a large fraction of D particles (on average: D:Be atomic ratio about 10%, some higher ratio up to 40% directly at the surface [39]). Compared to the LFS bulk-W, a much larger number of particles can be implanted within the HFS co-deposited layers on W-coated CFC PFCs due to larger porosity. Whereas in bulk-W a fluence of about $5 \cdot 10^{20}$ D m$^{-2}$ can be stored in the near-surface, the co-deposited layers of W-coated PFC can take up about $1 \cdot 10^{22}$ D m$^{-2}$ particle implantations which can be subsequently outgassed after heating up the PFC [19, 39].

Recently, in the JET-ILW campaigns in 2015/16 similar plasmas compared to the ones presented here (from 2012) have been executed ($I_p/B_t = 2.0$ MA/2.33 T, $P_{NBI} = 12$ MW, low-triangular semi-horizontal configuration with OSP on tile 5, the ISP located high or low on vertical tile 3). A fast acquisition camera system [40] with a sampling rate of up to 70 kHz capable in discriminating the areas emissions in the divertor (see figure 4) has been employed. From the data one can follow the sequence of events. Significant $D_\alpha$ emission has been observed close to the HFS co-deposited areas on tile 0/1 which is apparently due to surface heating during the ELM-crash (the latter identified in time with a BeII signal

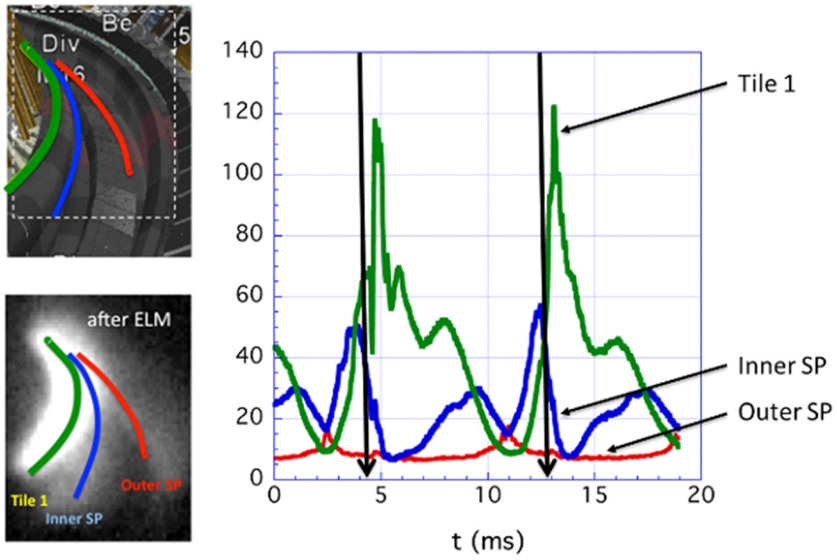


**Figure 4.** Fast camera signals (arb. units) of JET discharge #89372 disentangling $D_\alpha$ emission from outer (red) and inner divertor (blue) and on top of HFS tile 1 (green). The vertical arrows depict the BeII signal peak measured by spectroscopy in the HFS region which acts as a marker of the ELM event in time. During the ELM, the $D_\alpha$-emission on top tile 1 increases strongly and later decays within ~5–6 ms while the emission at the inner strike point region first decreases abruptly and later increases.

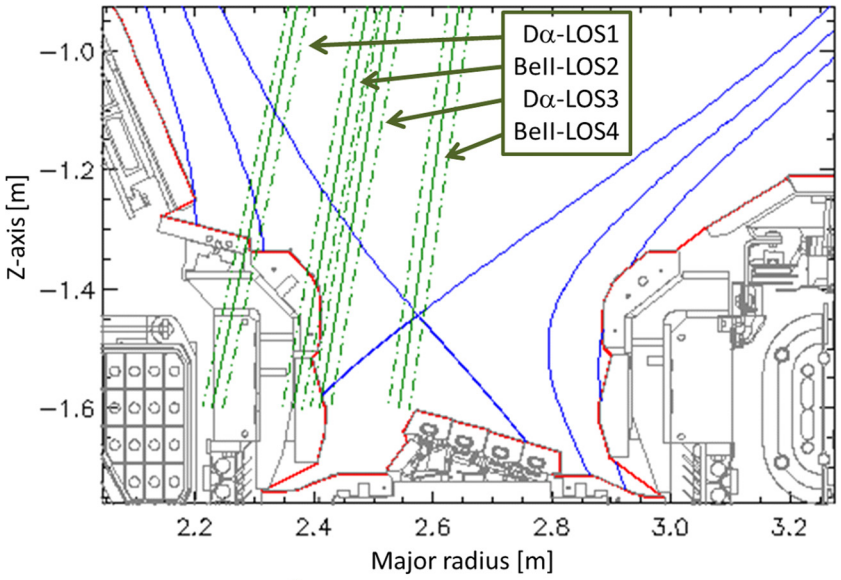


**Figure 5.** Lines-of-sight (LOS) of measured signals of selected sight lines of the KS3 visible divertor spectrometer of JET discharge #83712.

from spectroscopy). After the ELM the $D_\alpha$ emission on top tile 0/1 decays within ~6 ms. During this period the $D_\alpha$ emission increases slowly also near the bottom of the HFS divertor that peaks ~5 ms after the ELM crash. However the overall divertor emission is much weaker compared to the HFS top tile 0/1 emission. A small increase of the LFS divertor $D_\alpha$ signal is also observed that is even weaker than its HFS divertor counterpart.

As in this specific plasma discharge the ELM frequency $f_{\mathrm{ELM}}$ was about 120 Hz the sequence of events has been looked at by using visual spectroscopy for a different discharge with lower ELM frequency (see figures 5 and 6 for JET discharge #83712, taken from the identical plasma series described in section 3). Assuming again that the BeII signal can be seen as an identifier for a large ELM filament striking the plate one identifies a change of $f_{\mathrm{ELM}}$ during the discharge. At the beginning of the beam flattop phase the $f_{\mathrm{ELM}}$ is of the order 50 Hz whereas $f_{\mathrm{ELM}}$ decreases towards the end of the 6 s flattop phase of the same pulse to 20 Hz. It should be noted that the in the beginning of the NBI flattop phase the plasma is still in a transient phase before the plasma is found to be in dynamical equilibrium. The line averaged density increases by 25% from $4.3 \cdot 10^{19}$ m$^{-3}$ to $5.4 \cdot 10^{19}$ m$^{-3}$ and concomitantly, the ELM energy loss per ELM reduces from ~200 kJ to 160 kJ after 2 s in the flattop phase. From the total $D_\alpha$ emission in the inner and outer divertor one observes that the inter-ELM recycling flux increases in the transient

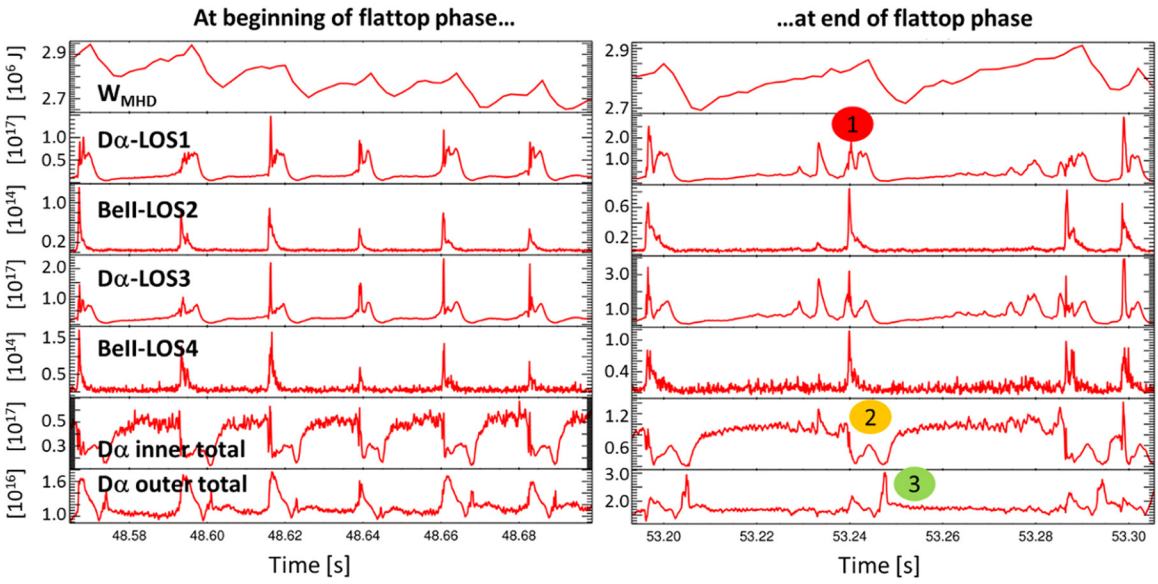


**Figure 6.** Time traces of measured $D_\alpha$ and BeII emission signals of the KS3 visible divertor spectrometer of JET discharge #83712 (see figure 5 for LOS), units (photons/(s cm$^2$ sr)). The $D_\alpha$ total signals are taken across all available lines-of-sights for the inner and outer target (not shown). The signal for $W_{MHD}$ ($10^5$ J) is lagging compared to the faster spectroscopy signal as the magnetic data acquisition is too slow. Left: set of signals at the beginning of the discharge flattop phase, right: the same but at the end of the 6 s flattop phase. For explanations of numbered markers on the right figure see the text.

phase by a factor 2 in the HFS and by 50% in the LFS. In the saturated phase the divertor inter-ELM recycling becomes slightly less asymmetric compared to the beginning of the NBI flattop phase.

From the visual spectroscopy depicted in figure 6 (right) pre-ELM precursors can be observed in the $D_\alpha$ light (on top of HFS baffle, inner and outer divertor) in the saturated phase of the discharge. These precursors apparently happen for all large ELMs in the late flattop phase of the discharge. In the same discharge at the beginning of the flattop phase these precursors however do not occur and the ELMs look 'clean'. Whether this feature can be related to increased MHD activity with increase in density is currently under investigation.

From the spectroscopic time traces one identifies the following structure in time after an ELM event in the late stage of the flattop phase (see figure 6, right): (1) a large $D_\alpha$ signal and thus recycling on top of HFS tile 1/0 (likely due to outgassing of heated co-deposited W-PFCs) with decay time ~6 ms, (2) followed by an increase of recycling in the HFS divertor (there $D_\alpha$ is reduced first at the ELM and peaks again 6 ms after), (3) followed by a secondary recycling peak 8 ms after ELM at the LFS divertor. A secondary $D_\alpha$ peak is also seen on top of tile 0/1 coinciding with the $D_\alpha$ peak at HFS divertor 6 ms after the ELM. Further analysis of this localized recycling process which is seemingly dependent on local conditions (local fluxes, surface conditions, i.e. $T_{surf}$, position of strike points) is still ongoing.

## 5. Conclusions

In contrast to JET-C, metallic devices as the JET-ILW exhibit a complex picture of the fueling process in type-I ELMy H-mode discharges. Particles have a significant larger kinetic reflectivity on metallic surfaces and thus the recycling process is much more susceptible to the selected divertor configuration. Without the omnipresence of a particle source from chemical sputtering of amorphous carbon layers at the wall the poloidal fueling profile is also much more affected by localized recycling effects.

In the investigated series of JET-ILW discharges with a semi-horizontal divertor configuration with a low triangular plasma shape, a long lasting and strong secondary $D_\alpha$ emission peak apparently stemming from D particles being outgassed in the HFS region from the Be co-deposits on tile 0/1 is observed. Particle retention in the HFS deposition region is understood to be much larger (up to 2 orders of magnitude in terms of fluence) due to larger porosity of the material. This HFS particle reservoir has the capability to store significantly more particles compared to the LFS bulk-W PFC. In the investigated semi-horizontal discharges the outgassing after an ELM from the HFS region is observed to be much stronger than from the LFS area with bulk-W PFCs. The localized HFS particle source can impact the poloidal fueling profile depending on the plasma clearance and/or available transported energy reaching the particle reservoirs in the far-SOL increasing $T_{surf}$. The localized recycling in the HFS decays on a time-scale of about 6 ms or more and adds up as an additional D particle fueling influx into the core due to its vicinity to the separatrix near and above the X-point. The extra influx after the ELM-crash from the HFS region is ultimately transported into the divertor where it is recycled and/or pumped away.

From the available data it is hard to disentangle the occurrence of a secondary recycling flux peak at the divertor plate occurring a few ms after the ELM burst as several processes happen at the same time on overlapping time-scales. Further statistical analysis is ongoing to discriminate the duration between the first and the second peak in $J_{sat}$ during an ELM burst, as well as the height of the secondary particle flux peak

to understand and see whether there is any correlation of delay time $\Delta t$ or height $\Delta h$ of the secondary recycling peak and of the local surface temperature $T_{surf}$ on the HFS and LFS regions

Usually, in vertical target or corner configuration the clearance to the HFS tile 0/1 region is larger. With less power reaching the far-SOL HFS region and with only moderate $T_{surf}$ increase (as seen regularly seen also from JET's protection cameras) a smaller number of particles is expected to be locally released and thus has a weaker effect on the poloidal fueling profile. However, it is again difficult to disentangle the various effects directly from experimental data as a vertical or corner divertor configuration also induces stronger pumping and the consequently fueling efficiency from divertor recycling is altered, too.

Similarity studies between DIII-D and Alcator C-mod have shown that the impact of fueling profile anisotropies is susceptible also to system size [41, 42]. In this view, an alternative hypothesis which has the potential to explain a secondary recycling peak after an ELM has been proposed by Wischmeier *et al* [43] which in principle follows the idea that a dynamical volumetric particle reservoir may lead to a retardation of pedestal recovery between ELMs due to lagged neutral transport within the divertor (including sub-divertor structures of the vessel). The observed time-scales of the time delay $\Delta t$ between primary and secondary recycling fluxes (~8 ms in JET-ILW, ~4 ms in AUG, and no observed secondary peak observed in smaller devices like Alcator C-mod) could perhaps indicate a possible size-scaling of $\Delta t$ assuming that the divertor volume scales at least linearly with major radius $R$.

Unfortunately, a direct and time-dependent measurement of the plasma and neutral flows in the SOL is not possible in JET. The full data set is to be taken to derive numerically the poloidal ionization and fueling profiles by using for example the SOLPS-ITER [23] or EDGE2D-EIRENE code packages [24, 25] to compare the H-mode fueling efficiency between JET-ILW and JET-C. By the time of writing the simulation attempts to take into account for example the extra fueling source like the additional HFS recycling shortly after the ELM from outgassing of Be co-deposits are still ongoing. In the near future the SOLPS-ITER is extended towards the inclusion of most of the aforementioned effects. Foreseen new features include (a) revised recycling models going beyond oversimplified reservoir models (e.g. [35]), i.e. a coupling to trap-diffusive models [31] into the EIRENE neutrals code monitoring also the evolution of surface temperatures in time for the bulk-W/W-coated CFC divertor tiles as well as for main-chamber Be PFCs and co-deposited areas, (b) extension of the plasma grid up to the first wall to improve model for global Be-erosion and migration towards co-deposition areas, (c) extension of the neutral grid into the sub-divertor to resemble any neutral buffering effects and thus recover volumetric particle reservoirs, (d) as for the JINTRAC model, a coupling to a core/pedestal code also for SOLPS-ITER simulations, and (e) general improvements for the pedestal transport models in such codes (e.g. coupling between density and temperature within the edge transport barrier). The impact of enhanced particle and energy reflectivity on the neutral kinetics effects is already included in the EIRENE code which is an essential part of the fluid-kinetic edge transport codes SOLPS-ITER [23] or EDGE2D-EIRENE [24, 25].

PWI including neutral recycling, penetration and transport alone are unlikely to determine the shape of the pedestal density profile and structure on their own as other mechanisms like MHD stability and pedestal transport are important drivers in the pedestal evolution. Recently, additional broadening mechanisms of the $p_{ped}$ with increase in collisionality $\nu^*_{ped}$ going beyond the $\sqrt{\beta_{pol,ped}}$ scaling have been identified [9, 44]. Currently, non-linear MHD and pedestal transport models are being revised to take such effects into account including also neutral recycling and transport [45].

## Acknowledgments

This work has been carried out within the framework of the EUROfusion Consortium and has received funding from the Euratom research and training programme 2014–2018 under grant agreement No 633053. The views and opinions expressed herein do not necessarily reflect those of the European Commission.

## References

[1] Matthews G.F. *et al* 2011 *Phys. Scr.* **T145** 014001
[2] Brezinsek S. *et al* 2015 *J. Nucl. Mater.* **463** 11–21
[3] Brezinsek S. *et al* 2013 *Nucl. Fusion* **53** 083023
[4] Philipps V. *et al* 2013 *J. Nucl. Mater.* **438** S1067
[5] Loarer T. *et al* 2015 *J. Nucl. Mater.* **463** 1117
[6] Wauters T. *et al* 2015 *J. Nucl. Mater.* **463** 1104
[7] De la Luna E. 2014 Comparative study of high triangularity H-mode plasma performance in JET with Be/W wall and CFC wall *Presented at 25th IAEA Int. Conf. on Fusion Energy (St. Petersburg)* [EC/P5-29]
[8] Joffrin E. 2014 Impact of divertor geometry on ITER scenarios performance in the JET metallic wall *Presented at 25th IAEA Int. Conf. on Fusion Energy (St Petersburg)* [EX/P5-40]
[9] Frassinetti L. *et al* 2017 *Nucl. Fusion* **57** 016012
[10] Snyder P.B. *et al* 2011 *Nucl. Fusion* **51** 103016
[11] Mahdavi M.A. *et al* 2003 *Phys. Plasmas* **10** 3984
[12] Groebner R.J. *et al* 2009 *Nucl. Fusion* **49** 085037
[13] Maggi C.F. *et al* 2015 *Nucl. Fusion* **55** 113031
[14] Groth M. *et al* 2013 *Nucl. Fusion* **53** 093016
[15] Brezinsek S. *et al* 2005 *Plasma Phys. Control. Fusion* **47** 615
[16] Guillemaut C. *et al* 2016 *Phys. Scr.* **T167** 014005
[17] Eckstein W. *et al* 2002 *Report IPP* 9/132
[18] Brezinsek S. *et al* 2016 *Phys. Scr.* **T167** 014076
[19] Mayer M. *et al* 2016 *Phys. Scr.* **T167** 014051
[20] Brezinsek S. *et al* 2015 *Nucl. Fusion* **55** 063021
[21] Borodkina I. *et al* 2016 An analytical expression for ion velocities at the wall including the sheath electric field and surface biasing for erosion modeling at JET ILW PSI submitted to NME
[22] Tamain P. *et al* 2015 *J. Nucl. Mater.* **463** 450
[23] Wiesen S. *et al* 2015 *J. Nucl. Mater.* **463** 480
[24] Simonini R. *et al* 1994 *Contrib. Plasma Phys.* **34** 368
[25] Wiesen S. *et al* 2006 *ITC Project Report* www.eirene.de/e2deir_report_30jun06.pdf
[26] Giroud C. *et al* 2015 *Plasma Phys. Control. Fusion* **57** 035004
[27] Balboa I. *et al* 2012 *Rev. Sci. Instrum.* **83** 10D530

[28] Frassinetti L. *et al* 2012 *Rev. Sci. Instrum.* **83** 013506
[29] Huber A. *et al* 2013 *Fusion Eng. Des.* **88** 1361
[30] Den Harder N. 2016 *Nucl. Fusion* **56** 026014
[31] Schmid K. *et al* 2016 *Phys. Scr.* **T167** 014025
[32] Sugiyama K. *et al* 2014 *Phys. Scr.* **T159** 014043
[33] Schmid K. *et al* 2016 *Presentation at DivSOL ITPA Meeting (Naka, Japan, October 2016)*
[34] Romanelli M. *et al* 2014 *Plasma Fusion Res.* **9** 3403023
[35] Wiesen S. *et al* 2016 *Contrib. Plasma Phys.* **56** 754
[36] de la Luna E. 2016 Recent results on high-triangularity H-mode studies in JET-ILW *Preprint: 2016 IAEA Fusion Energy Conf. (Kyoto)* [EX/P6-11]
[37] Scott B. *et al* 2016 *Contrib. Plasma Phys.* **56** 534
[38] Widdowson A. 2017 Overview of fuel inventory in JET with the ITER-like wall *Nucl. Fusion* submitted
[39] Heinola K. 2017 Long-term fuel retention and release in JET ITER-like wall at ITER relevant baking temperatures *Nucl. Fusion* submitted
[40] de la Cal E. *et al* 2012 *Proc. 39th EPS Conf. on Plasma Physics (Stockholm, Sweden)*
[41] Hughes J.W. *et al* 2007 *Nucl. Fusion* **47** 1057
[42] Groebner R.J. *et al* 2013 *Nucl. Fusion* **53** 093024
[43] Wischmeier M. *et al* 2007 *J. Nucl. Mater.* **363–5** 448
[44] Maggi C. 2017 Studies of the pedestal structure in JET with the ITER-like wall *Nucl. Fusion* submitted
[45] Pamela S. 2017 Multimachine modelling of ELMs and pedestal confinement: from validation to prediction *Nucl. Fusion* submitted
[46] Harting D. *et al* 2015 *J. Nucl. Mater.* **463** 493
[47] Jaervinen A. *et al* 2016 *Nucl. Fusion* **56** 046012